

# Materials Science

An Indian Journal

Full Paper

MSAIJ, 14(3), 2016 [088-099]

## Investigation of structural changes during recovery of crystal defects in plastically deformed Fe<sub>50</sub>Ni<sub>50</sub> alloy by magnetic measurements

A.R.Ali, F.Z.Ghobrial, E.Takla\*, K.K.Meleka

Physics Department, Faculty of Science, Cairo University, Giza, (EGYPT)

E-mail: eman.takla@yahoo.com

### ABSTRACT

In the present work, the behavior of structural changes during recovery of crystal defects in plastically deformed Fe<sub>50</sub>Ni<sub>50</sub> alloy by magnetic measurements is investigated. Isochronal annealing experiments in the temperature range from 25 to 900 °C revealed the existence of different annealing stages in the annealing spectrum of plastically deformed Fe<sub>50</sub>Ni<sub>50</sub> alloy. The first stage appeared around 225 °C activated by  $1.08 \pm 0.015$  eV which is explained based on an increase in local order in the alloy matrix. The second stage detected in the temperature range from 550 to 750 °C arises because of the dissociation of defect clusters activated by  $1.85 \pm 0.013$  eV. The third recovery stage appeared above 750 °C activated by  $3.03 \pm 0.06$  eV, and the process is related to be the climb motion of dislocations during the recrystallization process. Changes in initial lattice defect concentration are found to have influence on the observed stages. The kinetics of FeNi<sub>3</sub> precipitation observed at high temperature ( $T_a < 800$  °C) are observed.

© 2016 Trade Science Inc. - INDIA

### KEYWORDS

Fe<sub>50</sub>Ni<sub>50</sub>;  
Ferromagnetic alloy;  
Magnetic properties;  
Plastic deformation;  
Activation energy;  
Order of reaction.

### INTRODUCTION

Attention has recently been focused on the behavior of recovery of lattice defects in deformed stainless steel, Fe-based and perm alloys. These alloys were an important class of materials for present and future technological applications<sup>[1-14]</sup>. Actually, the structure sensitive properties of these materials were directly dependent on such fundamental processes as creation of lattice defects, defect diffusion, and defect reaction in the alloy matrix. On the other hand, several authors<sup>[15-17]</sup> observed the changes in the structural sensitive properties of Fe-based alloys during the annealing of irradiated or

cold-worked alloys above room temperature. Results of some of those experiments were explained based on either solute segregation; changes in short-range order; or precipitation of ordered phases. These processes cause microscopic homogeneities in the alloy matrix, which lead to anomalous changes in the physical property, measured. Moreover, the present binary alloy Fe<sub>50</sub>Ni<sub>50</sub> of superstructure L1<sub>2</sub> type (Ni<sub>3</sub>Fe)<sup>[18]</sup>, its prospect as soft magnetic material and good corrosion resistance<sup>[19,20]</sup> at elevated temperature were of additional interest. This binary system forms a long range ordered intermetallic phase with superstructure L1<sub>2</sub> type (Ni<sub>3</sub>Fe), which has FCC unit cell with Fe atoms occupy the corners

and Ni atoms occupy the middle of the faces of the cube<sup>[21]</sup>. While in the disordered phase, Ni and Fe atoms randomly occupy the FCC lattice sites. According to the constitution diagram of Fe-Ni alloy<sup>[21]</sup> the ordered and disordered phases coexist in equilibrium around 557 °C, while below this temperature the ordered phase is stable. Therefore, it is expected that the annealing behavior of the physical parameters of intermetallic compounds after cold-worked, is more complex than in pure metals or solid solution alloys, there exists a restriction imposed on the formation and movements of vacancies. This restriction is due to the thermal formation of vacancies on the two sublattices, concomitant thermal formation of antisite defects on both sublattices, and the coexistence of point defects due to deviations from the stoichiometric composition<sup>[22,23]</sup>. Therefore, it is expected that the annealing behavior of the physical parameters of intermetallic compounds after cold-worked are more complex than in pure metals. On the other hand, since in intermetallic compounds the local order transformation caused by short-range or long-range ordering are induced by diffusion of point defects. Therefore, it was difficult to separate ordering effects from those due to vacancy or interstitial annealing. Although several studies<sup>[23-25]</sup> have been made on the thermal formation and migration of point defects in intermetallic compounds by various techniques, fundamental information on the temperature and composition dependence of point defects is still remains a challenging problem. The magnetic structure sensitive properties measured in this work, such as the maximum magnetic permeability ( $\mu_{\max}$ ) and the magnetic coercivity ( $M_{cr}$ ) were highly defect specific and they can be used to study the formation sequence and relative stability of corresponding microstructure configuration in intermetallic Fe<sub>50</sub>Ni<sub>50</sub> alloy. The aim of the present work is to study the behavior of recovery of lattice defects and their interaction in cold-worked Fe<sub>50</sub>Ni<sub>50</sub> alloy. It is hoped to gather some information about the different atomic mechanisms responsible for the release

of stored energy from cold-worked Fe<sub>50</sub>Ni<sub>50</sub> alloy during the different recovery stages above room temperature

## EXPERIMENTAL PROCEDURE

The under investigation material, Fe<sub>50</sub>Ni<sub>50</sub> alloy, is prepared from high purity Fe and Ni by induction melting followed by a suitable homogenization at 1200 °C under a helium atmosphere for 24 hours, then slowly cooled to room temperature. The material shaped by extrusion into rods of 3 mm diameter followed by swaging at room temperature to wires of 1 mm diameter.

The chemical composition of the prepared Fe<sub>50</sub>Ni<sub>50</sub> alloy is determined using atomic absorption method and tabulated in TABLE 1<sup>[26]</sup>. The wire sample is introduced as the core of a magnetization coil and the cathode ray technique is employed to obtain room-temperature B-H curves at different magnetizing fields. The maximum magnetic permeability is obtained from the relation  $\mu_{\max} = (B/H)_{\max}$ , which characterizes the magnetization of both reversible and irreversible domain-wall motion. Plastic strain deformation is induced on the samples by a locally conventional strain machine. The different degrees of plastic strain deformation are measured by the dimensionless quantity  $\eta\% = \Delta L/L\%$  where  $\Delta L$  and  $L$  are the change in length and the initial length of the sample, respectively<sup>[27]</sup>.

A cylindrical non-inductive furnace of length 30cm and diameter 9cm with heater wire uniformly distributed along its length is used. A silica glass tube is inserted containing the specimen, and the temperature inside the furnace was constant along its middle third of its length and could be maintained constant for several hours to within  $\pm 2^\circ\text{C}$ . After giving the samples prescribed annealing pulses the silica tube container was taken out from the furnace and left in air to cool to room temperature. Isochronal annealing is used to study the structural changes during recovery of plastically deformed of Fe<sub>50</sub>Ni<sub>50</sub> al-

TABLE 1 : Chemical composition of Fe<sub>50</sub>Ni<sub>50</sub> alloy

Fe	Ni	Mn	Zn	Mg	Sn	Al	Cu
Major	Major	-	0.001	-	0.001	0.001	0.001

Full Paper

loy. In isochronal annealing, the sample is heated for a constant time at different increasing temperatures. Care is taken during cooling from the curve annealing temperature and in the subsequent reheating to control the rate of temperature changes, so that it was never so great to cause further plastic

deformation.

RESULTS

Isochronal recovery data of cold-worked Fe<sub>50</sub>Ni<sub>50</sub> alloy

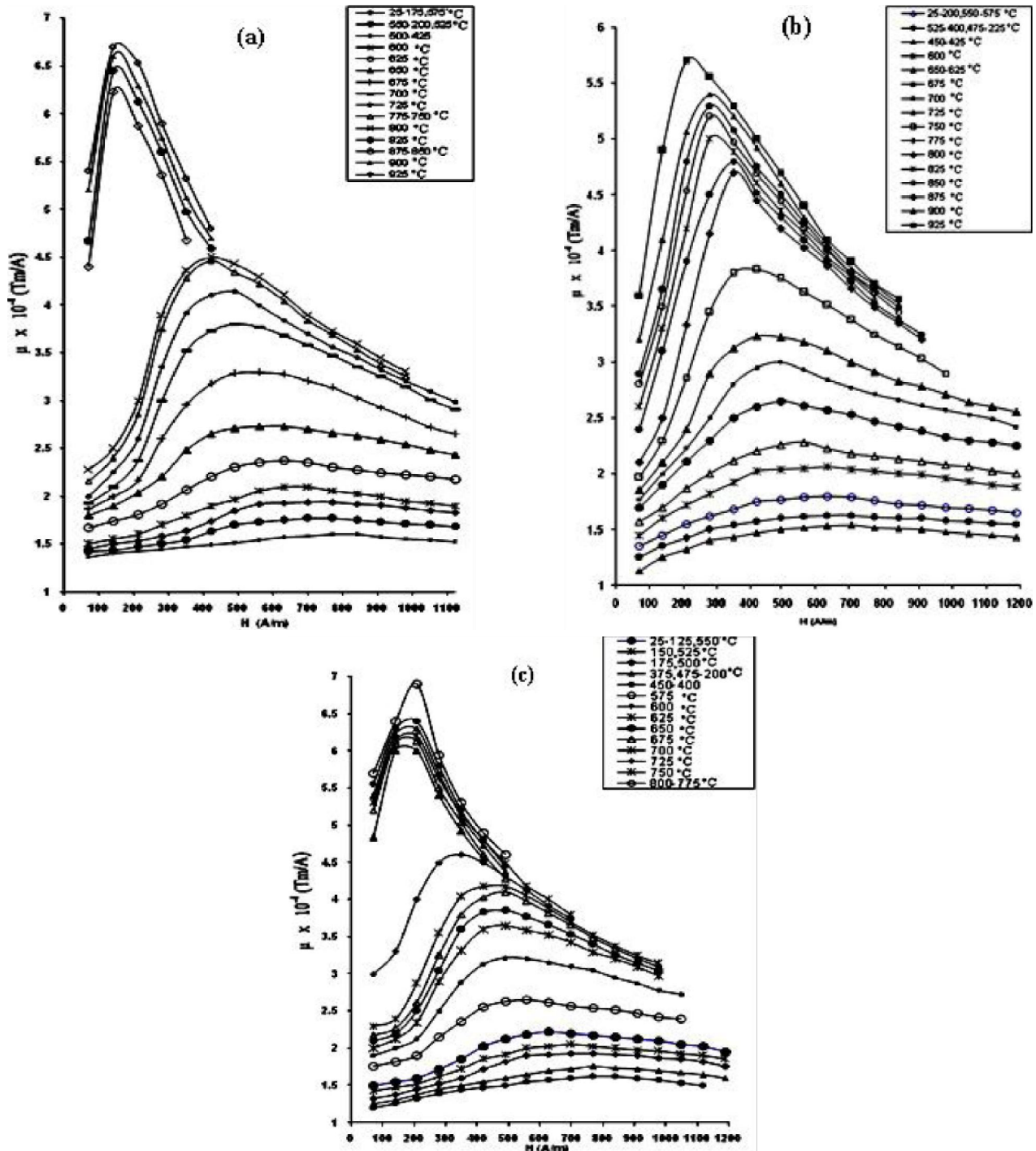


Figure 1 : Effect of isochronal annealing temperature on the dependence of the magnetic permeability  $\mu$ , on the magnetic field  $H$ , of deformed Fe<sub>50</sub>Ni<sub>50</sub> sample. (a)  $\eta = 6\%$ ,  $t_a = 10$  minutes, (b)  $\eta = 9.5\%$ ,  $t_a = 10$  minutes, and (c)  $\eta = 12\%$ ,  $t_a = 10$  minutes

Sets of isochronal annealing curves were obtained in the temperature range from 25 to 925°C of different cold-worked Fe<sub>50</sub>Ni<sub>50</sub> alloy ( $\eta = 6, 9.5, 12\%$ ), showing the variation of magnetic permeability with the annealing temperatures (Figure 4.1a-c). The curves are characterized by pronounced peak values in the magnetic permeability. These peaks shifted their positions to a lower or higher magnetic field depending on the annealing state of the sample.

The maximum magnetic permeability ( $\mu_{\max}$ ) was obtained from the relation  $\mu_{\max} = (B/H)_{\max}$ , which characterizes the magnetization of both reversible and irreversible domain wall motion, while the critical magnetic field ( $H_{cr}$ ) was obtained from the peak position of  $\mu_{\max}$  (Figure 1). The maximum magnetic permeability ( $\mu_{\max}$ ) has the advantage to provide sufficient sensitivity for samples of small ferromagnetic volume and shows high structural sensitivity if one compares it with other magnetic properties. Therefore, our present experimental results have been reported in normalized form of maximum magnetic permeability, namely, the fraction

$$K = \frac{|\mu_{\max}(T_a) - \mu_{\max}(i)|}{|\mu_{\max}(f) - \mu_{\max}(i)|} = \frac{\Delta\mu_{\max}(T_a)}{\Delta\mu_{\max}(0)}$$

has been used, where: (i) is the initial value of the maximum magnetic permeability before

annealing,  $\mu_{\max}(T_a)$  and  $\mu_{\max}(f)$  are the values after annealing temperature ( $T_a$ ) and the value after final high temperature anneal, respectively (all measurements were carried at room temperature).

Figure 2a shows the relative changes in the maximum magnetic permeability of three different plastically deformed samples ( $\eta = 6, 9.5$  and  $12\%$ ) after isochronal annealing by heat pulses of 10 minutes. It revealed the presence of three annealing stages, stage I, stage II and stage III in the temperature range 25–950 °C.

The relative changes in the maximum magnetic permeability exhibit a small decrease in the temperature range from 150 to 300 °C (stage I), leading to maximum magnetic permeability values smaller than that measured after plastic deformation. This stage is followed by a large increase in the maximum magnetic permeability which can be subdivided into two stages, stage II (from 400 to 750 °C) and stage III (from 750 to 850 °C). A final decrease in the maximum magnetic permeability is only observed for high deformed samples ( $\eta = 9.5$  and  $12\%$ ) above 850 °C. The demonstration of these annealing stages could be made better distinguishable by plotting the annealing spectrum of the maximum magnetic permeability as depicted in Figure 2b.

It is clear that increasing the initial defect con-

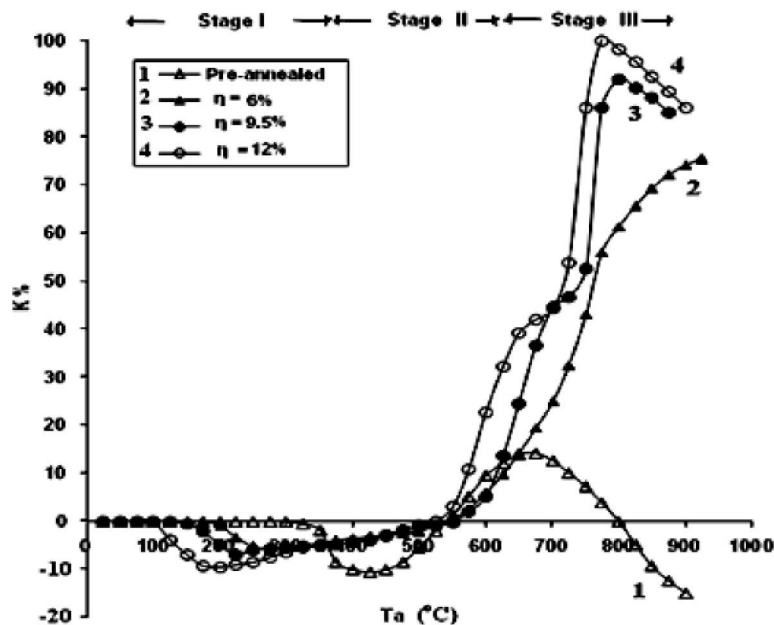


Figure 2a : The relative change of maximum magnetic permeability  $K = [\Delta\mu_{\max}(0)/\Delta\mu_{\max}(T_a)]$  with annealing temperature,  $T_a$  of: (1) pre-annealed Fe<sub>50</sub>Ni<sub>50</sub> sample, (2) deformed Fe<sub>50</sub>Ni<sub>50</sub> sample ( $\eta = 6\%$ ), (3) deformed Fe<sub>50</sub>Ni<sub>50</sub> sample ( $\eta = 9.5\%$ ) and (4) deformed Fe<sub>50</sub>Ni<sub>50</sub> sample ( $\eta = 12\%$ )

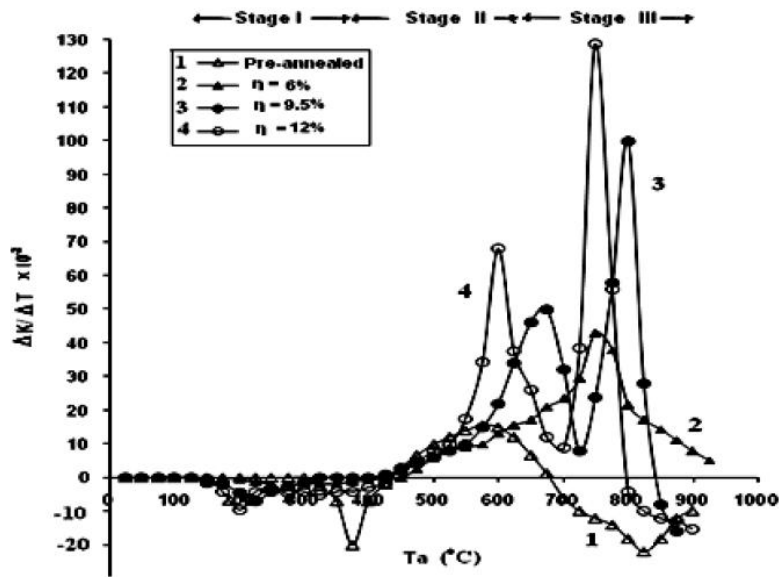


Figure 2b : The annealing spectrum of maximum magnetic permeability with annealing temperature  $T_a$  of: (1) pre-annealed  $Fe_{50}Ni_{50}$  sample, (2) deformed  $Fe_{50}Ni_{50}$  sample ( $\eta = 6\%$ ), (3) deformed  $Fe_{50}Ni_{50}$  sample ( $\eta = 9.5\%$ ), and (4) deformed  $Fe_{50}Ni_{50}$  sample ( $\eta = 12\%$ )

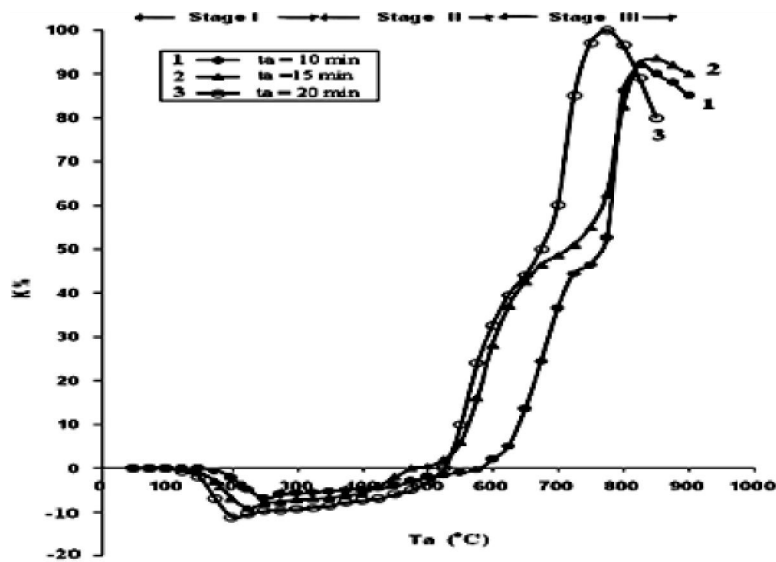
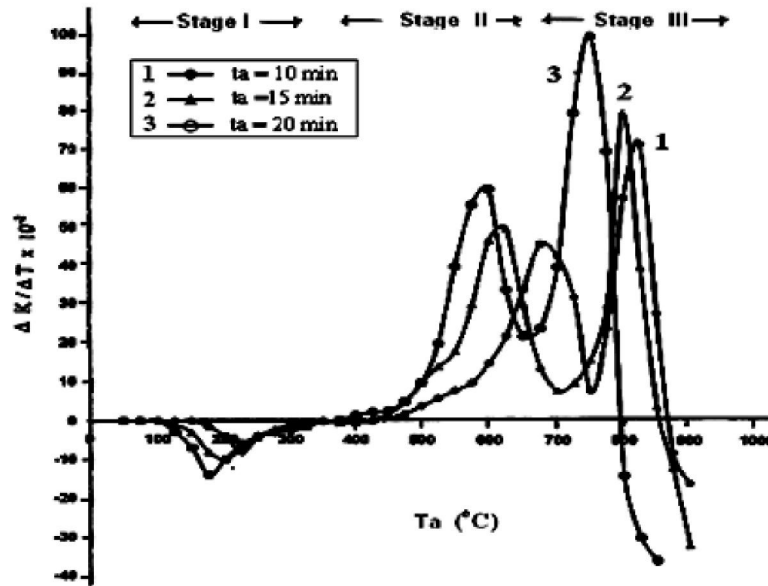


Figure 3 : The relative change of maximum magnetic permeability  $K = [\Delta\mu_{max}(0)/\Delta\mu_{max}(T_a)]$  with annealing temperature  $T_a$  of deformed  $Fe_{50}Ni_{50}$  sample ( $\eta = 9.5\%$ ) at different annealing times: (1)  $t_a = 10$  minutes, (2)  $t_a = 15$  minutes, and (3)  $t_a = 20$  minutes

centration by increasing the degree of plastic deformation modifies the amplitude and the position of different annealing stages. It is clear also that the final decrease in the maximum magnetic permeability is observed at high temperature for high deformed sample ( $\eta = 9.5$ , and  $12\%$ ) is not appeared during isochronal annealing of low deformed samples ( $\eta = 6\%$ ) (Figure 2b).

The relative change in the maximum magnetic permeability,  $k$ , for three plastically deformed

$Fe_{50}Ni_{50}$  alloy with the same degree of plastic deformation ( $\eta = 9.5\%$ ) with three different heat times of annealing ( $t_a = 10, 15$ , and  $20$  minutes) are represented in Figure 3. It is observed that the general behavior of the annealing spectrum is the same in the three samples, while the amplitude and the position of the different annealing stages depend on the heat pulse of the isochronal annealing (Figure 3 and Figure 4).



**Figure 4 :** The annealing spectrum of maximum magnetic permeability  $K = [\Delta\mu_{\max}(0)/\Delta\mu_{\max}(T_a)]$  with annealing temperature  $T_a$  of deformed  $\text{Fe}_{50}\text{Ni}_{50}$  sample ( $\eta = 9.5\%$ ) at different annealing times: (1)  $t_a = 10$  minutes, (2)  $t_a = 15$  minutes, and (3)  $t_a = 20$  minutes

### Activation energy and the annealing kinetics

Quantitative information on the recovery behavior and annealing kinetics of deformed  $\text{Fe}_{50}\text{Ni}_{50}$  alloy are obtained by calculating the activation energy ( $E$ ) and the order of reaction ( $\gamma$ ) associated with the corresponding observed recovery stages. Both values were determined using the isothermal annealing curves of the maximum magnetic permeability (Figure 5). Equivalent times and temperatures characterizing the annealing processes are found by using the cross-cut method and the energies activating the processes concerned for the three stages I, II and III were calculated (Figure 6). Furthermore, the order of reaction ( $\gamma$ ) was calculated from isothermal annealing curves for stages I, II and III. Following treatment previously adopted by Damask and Dienes<sup>[28]</sup> (Figure 7), and by Meechan and Brinkman<sup>[29]</sup> (Figure 8a-c and TABLE 2).

The activation energy by using other different methods such as Meechan-Brinkman method<sup>[39]</sup> and peak position method, can be determined (Figures 9, 10 and 11).

## DISCUSSION AND CONCLUSION

The results of the isochronal annealing observed in the present work in cold-worked  $\text{Fe}_{50}\text{Ni}_{50}$  alloy,

in the temperature range from 125 to 900 °C (Figure 1a-c) are quite different from those previously reported for cold-worked,  $\alpha\text{-Fe}$ <sup>[30,31]</sup> and some Fe-alloys<sup>[31,32]</sup>. In the present work, the anomalous change in  $\mu_{\max}$  and  $H_{cr}$  in the temperature range 125-500 °C (stage I) could not be ascribed to the annihilation of lattice defects induced by cold-worked. It could be explained on the basis of either solute segregation, changes in short-range order, or precipitation of ordered phase<sup>[33,34]</sup>. The above processes cause microscopic inhomogeneities leading to an increase in the internal stress in the alloy matrix<sup>[35]</sup>. This is expected to increase the density of pinning sites for the motion of magnetic domain walls in the matrix, resulting in the increase of  $H_{cr}$  and the decrease of  $\mu_{\max}$  beyond the pre-annealed value (Figures 2b and 3b). Beside, the structural change by short-range order has been assigned by most workers to the migration of either self-interstitial atoms as well as that of vacancies<sup>[33,36]</sup>. In the present work, since the isochronal annealing during stage I is continued over the whole temperature range from 125 to 500°C, therefore, the interstitial atoms migration could be definitely excluded in this temperature range<sup>[37]</sup>. From this consideration, stage I could be attributed the structural change in the alloy matrix by short-range ordering promoted by migration of vacancies, formed

## Full Paper

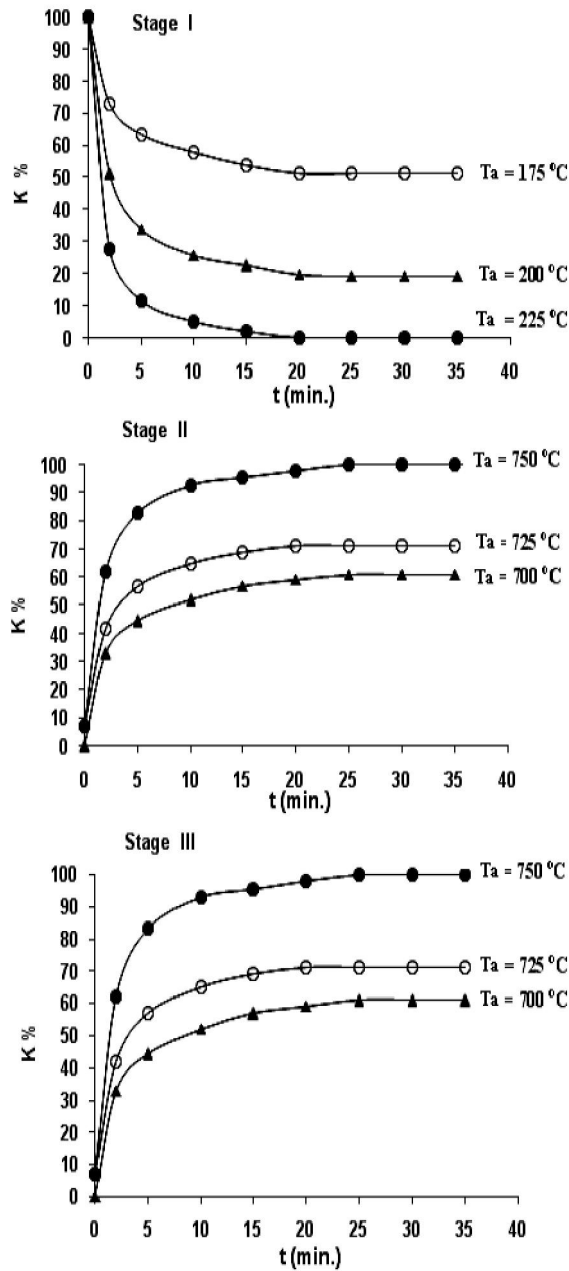


Figure 5 : Isochronal annealing of the maximum magnetic permeability of deformed  $\text{Fe}_{50}\text{Ni}_{50}$  sample in different annealing stages I, II and III ( $\eta = 9.5\%$ )

by plastic deformation  $\text{Fe}_{50}\text{Ni}_{50}$  alloy to deep traps or sinks. During isochronal annealing of the disordered  $\text{Fe}_{50}\text{Ni}_{50}$  alloy of structure below equilibrium level, each vacancy jump induced a certain increase of local order. This corresponds to a decrease in  $\mu_{\text{max}}$  and an increase in  $H_{\text{cr}}$ . The contribution of vacancy migration, leading to an increase in short-range order, has also been suggested by Sharma et al.<sup>[38]</sup> and Nakata et al.<sup>[39]</sup> in annealing studies of irradiated Fe-Cr-Ni alloy. These evidences suggest that

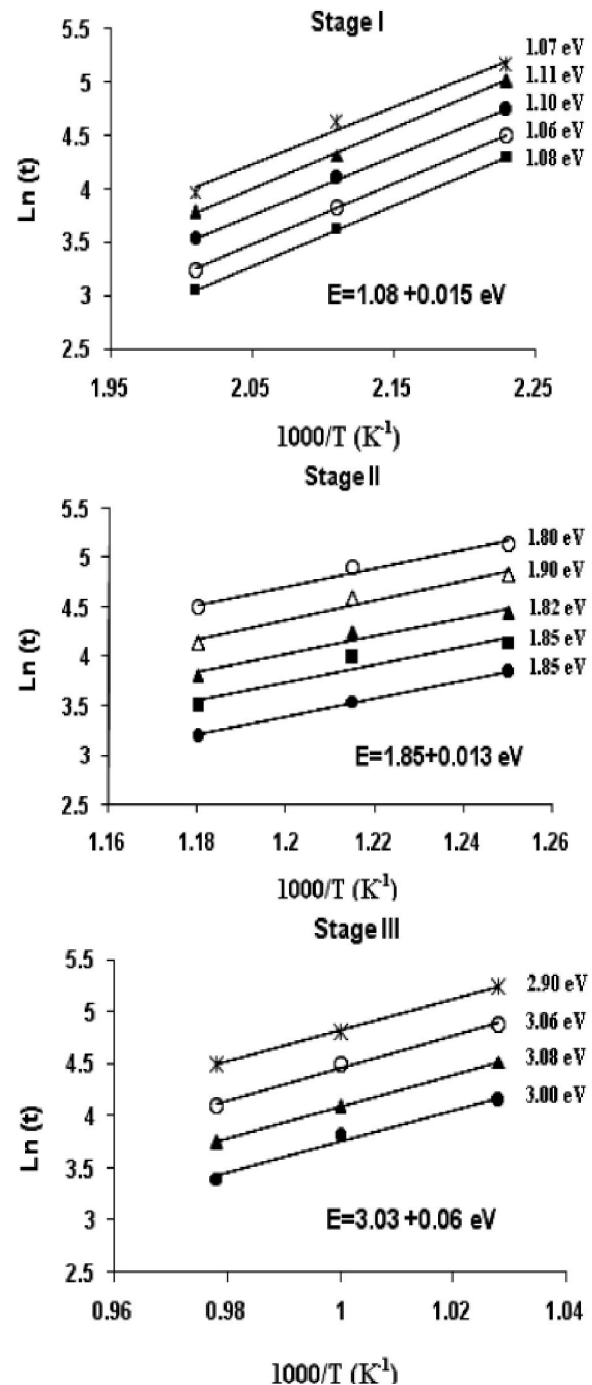


Figure 6 : Activation energies of the three stages I, II and III of deformed  $\text{Fe}_{50}\text{Ni}_{50}$  sample using the cross cut method ( $\eta = 9.5\%$ )

in the present stage (stage I) the anomalous change in  $\mu_{\text{max}}$  and  $H_{\text{cr}}$  is due to the change in the local order produced by the long-range migration of vacancies. When the vacancy become mobile, it performs a certain number of jumps before annihilation or trapping in clusters and can promote the evolution of the local atomic order of the alloy towards its equilib-

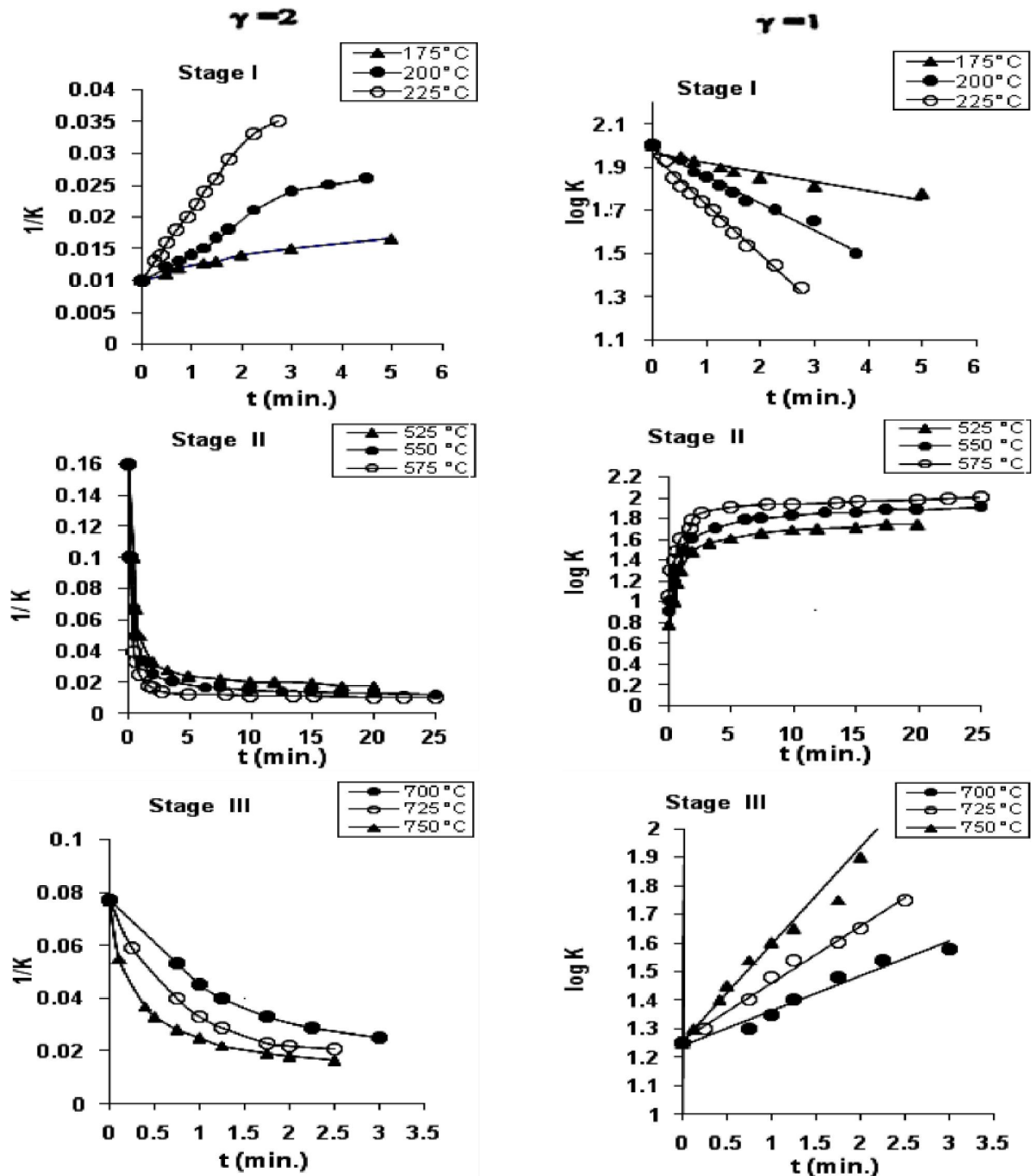


Figure 7 : Determination the order of reaction for stages I, II and III of cold-worked Fe<sub>50</sub>Ni<sub>50</sub> alloy using damask and dienes method

rium state. The presently determined activation energy of stage I ( $1.06 \pm 0.02$  eV) is of the same order of magnitude as that required for free mono-vacancy migration in  $\alpha$ -Fe [30,31]. Beside, the annealing process during this stage is controlled by reaction kinetics of an order greater than one (Figures 7 and

8). These results support the idea that the change in structural ordering by short-range order is controlled by free vacancy migration, with the possible formation of vacancy clusters or complex aggregates [30,31]. Further during isochronal annealing of undeformed (pre-annealed) sample (Figure 2b), the maximum

## Full Paper

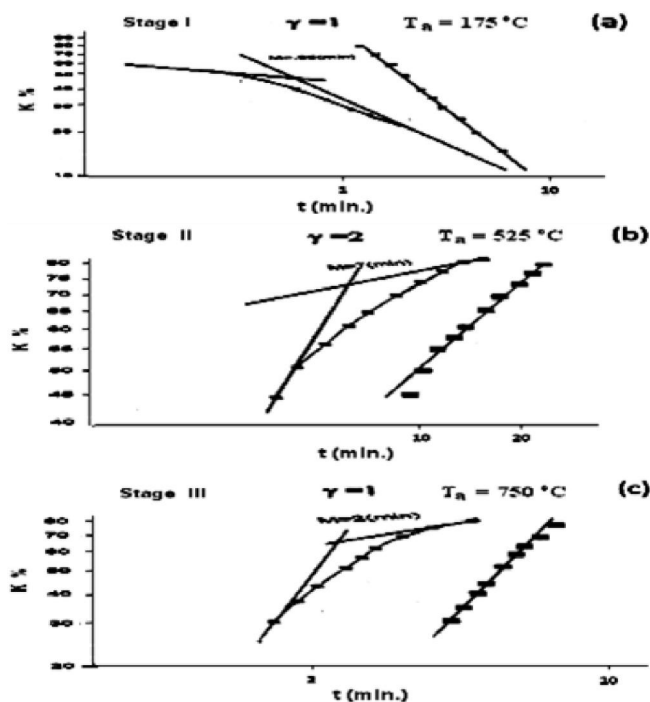


Figure 8 : Determination the order of reaction for stages I, II and III of cold-worked  $\text{Fe}_{50}\text{Ni}_{50}$  alloy using Meechan-Brinkman method: (a) stage I, (b) stage II, and (c) stage III

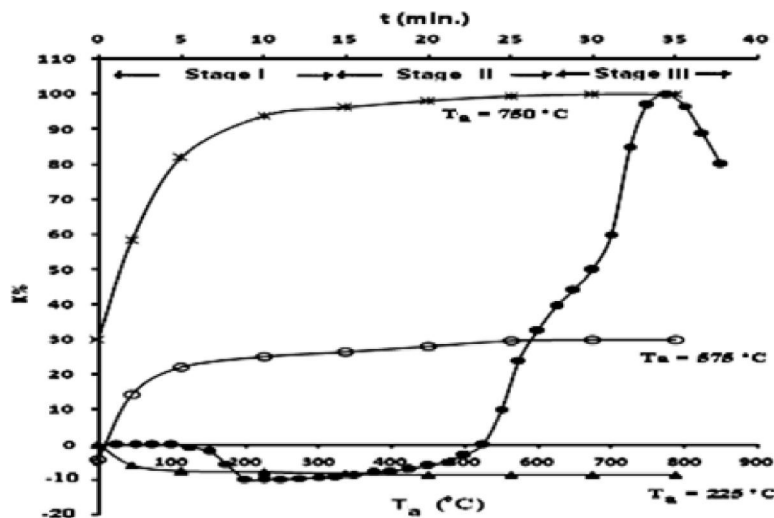


Figure 9 : Isothermal and isochronal annealing curves of the maximum magnetic permeability of cold-worked  $\text{Fe}_{50}\text{Ni}_{50}$  alloy

magnetic permeability ( $\mu_{\max}$ ) remains constant in the temperature range from 25 to 350 °C. This is because the diffusion rate of thermal vacancies and their concentration are not enough to cause a change in the atomic order up to 370 °C. While at higher temperature, above 375 °C, the maximum magnetic permeability starts decreasing up to 550 °C, where the effect of thermal vacancy diffusion becomes ap-

preciably in Fe-alloy<sup>[19]</sup>. Therefore the observed decrease in  $\mu_{\max}$  during isochronal annealing of undeformed (pre-annealed) sample in the temperature range from 375 to 550 °C is caused by the diffusion of thermal vacancies created during thermal treatment and can promote the evaluation of the local atomic order of the alloy towards its equilibrium state. Finally, the observed variation in both the amplitude and the shift in position of this stage towards lower annealing temperature with increasing the degree of plastic deformation (Figure 2b) could be reasonably related to the initial increase in the concentration of vacancies in the alloy matrix with increasing the degree of plastic deformation. Therefore, the increase in concentration of vacancies would enhance the change in local order by short-range ordering during this stage. The second annealing stage (stage II), centered around 600 °C, showing up, as an increase in  $\mu_{\max}$  is associated with a decrease in  $H_{cr}$ . This annealing stage observed in the present work in cold-worked, quenched and laser damaged samples (Figures.2b and 3b) could be

attributed to the dissociation of vacancy clusters or complex aggregates formed during stage I, resulting in a release of free mono-vacancy. The vacancy migrates further to a deeper trap or falls into sinks during the migration process with annealing temperature rising from 550 to 750 °C. This process is expected to decrease the density of the load on the magnetic domain walls. Hence, an increase in  $\mu_{\max}$

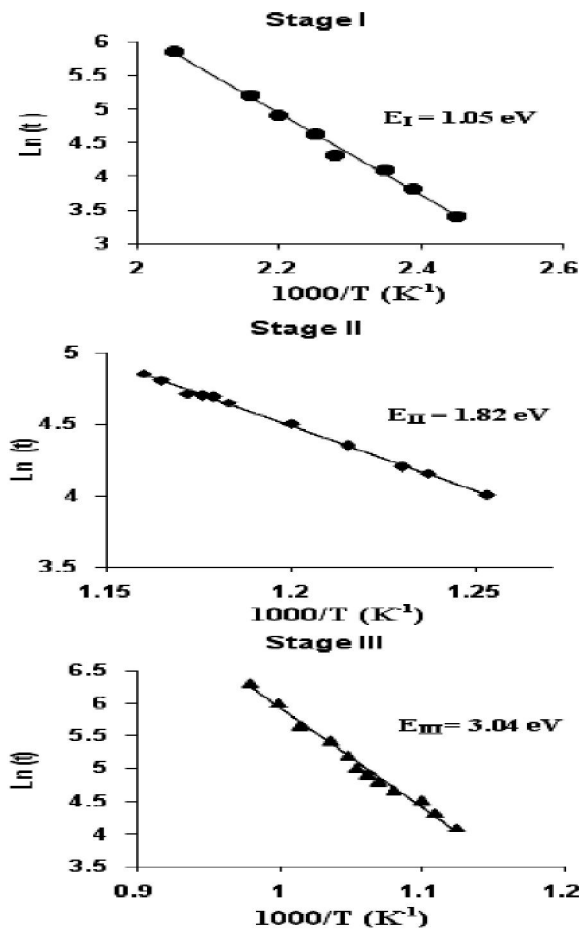


Figure 10 : The activation energies for the three stages I, II and III of deformed  $Fe_{50}Ni_{50}$  sample ( $\eta = 9.5\%$ ) using meechan-brinkman method

together with a drop in  $H_{cr}$  is observed during this annealing stage (Figures 2b and 3b). The presently determined activation energy of this stage ( $1.8 \pm 0.01$  eV) had the same order of magnitude as that required for the dissociation of vacancy clusters in Fe and Ni alloys<sup>[41,42]</sup>. Moreover, the recovery process during this stage is largely controlled by a second order reaction kinetics (TABLE 2). This implied that this stage of recovery might be due to a bimolecular reaction, presumably the dissociation of vacancy clusters, formed during the first stage, by normal self-diffusion of vacancies<sup>[30]</sup>. Beside, the observed shift of stage II towards lower annealing temperature with increasing the degree of plastic deformation (Figure 2b) could be reasonably related to the increase in vacancy cluster content in the alloy matrix formed at the end of stage I. This is actually related to the increase in the concentration of vacancies in the alloy matrix with increasing the degree plastic deforma-

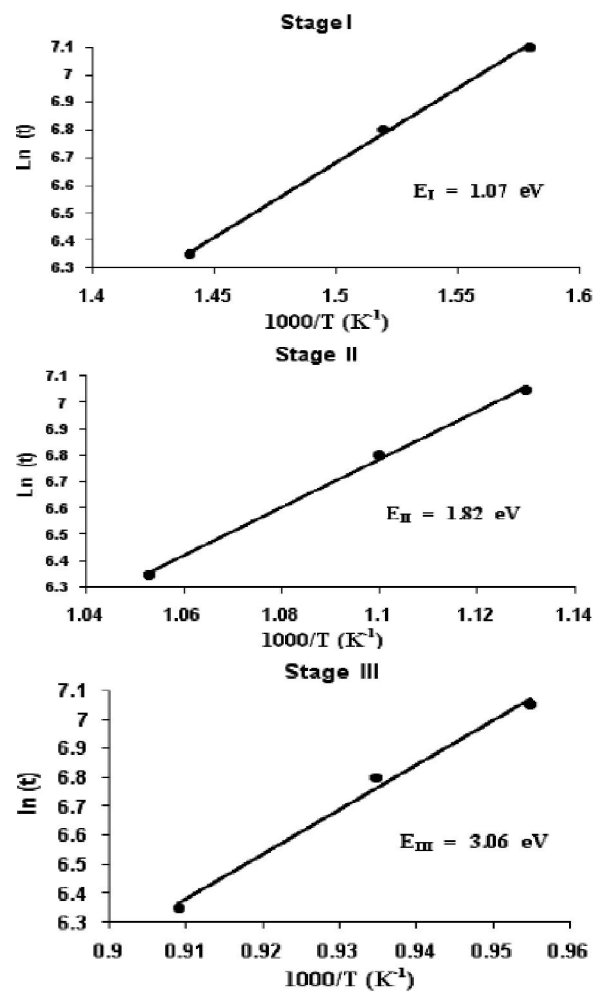


Figure 11 : The activation energies for the three stages I, II and III of deformed  $Fe_{50}Ni_{50}$  sample ( $\eta = 9.5\%$ ) using peak position method

tion, and as expected, this would enhance the mechanism responsible for the annealing process during stage II in cold-worked samples.

The higher temperature annealing stage (stage III) observed in the present work only during the isochronal annealing of cold-worked  $Fe_{50}Ni_{50}$  alloy in the temperature range from 750 to 825 °C could be attributed to a recrystallization phenomenon. As expected, the amplitude of this stage increases and its position shifts to lower annealing temperature with increasing the degree of plastic deformation (Figure 2b). The observed increase of  $\mu_{max}$ , when recrystallization started in the deformed alloy matrix, was thought to be due to the release of some of the dislocations forming the cell boundaries through a process of climb by edge dislocation<sup>[43]</sup>. The subsequent removal of these dislocations settles down the den-

## Full Paper

**TABLE 2 : Represents the activation energy and the order of reaction for different recovery stages using different methods**

Stage	Activation energy (eV)			Order of reaction ( $\gamma$ )
	Cross-cut method	Meechan -Brinkman method	Peak position method	
I	1.08±0.015	1.05	1.07	1
II	1.85±0.013	1.82	1.82	2
III	3.03±0.06	3.04	3.06	1

sity of pinning sites for the motion of magnetic domain walls in the matrix, which consequently decrease the load on the magnetic domain. Hence, a continuous decrease in  $H_{cr}$  associated with an increase in  $\mu_{max}$  is observed in this annealing stage (Figures 2b and 3b). As mentioned earlier, the controlling process in the annealing stage is climb, which is essentially as self-diffusion mechanism. This process should give first-order kinetics that is actually observed in this stage (TABLE 2). Moreover, since dislocation climb is associated with mass transport, the activation energy for this annealing process should be of the order of magnitude of that for self-diffusion<sup>[41,42]</sup>. The experimental value of the activation energy ( $3.06 \pm 0.02$  eV) obtained in the present work (TABLE 2) for recrystallization in cold-worked Fe<sub>50</sub>Ni<sub>50</sub> alloy is in good agreement with previously published data for self-diffusion energy in the ferromagnetic materials<sup>[30,43]</sup>.

Finally, the observed decrease in the maximum magnetic permeability in all samples (pre-annealed and cold-worked), in the temperature range from 825 to 900 °C (Figures 2b and 3b) is most probably due to the precipitation of FeNi<sub>3</sub> phase<sup>[43,44]</sup>. The precipitation of this phase causes a marked expansion of the material, leading to an increase in the dislocation density in the alloy matrix<sup>[43,44]</sup>. This process seemed to impose a heavily pinning action on the magnetic domain walls, preventing them from normal detachment from fixation points and leak out the magnetic pressure exerted by the magnetic field on domain walls<sup>[31,32]</sup>. This effect tends to decrease the maximum magnetic permeability, which is actually observed during isochronal annealing of cold-worked Fe<sub>50</sub>Ni<sub>50</sub> alloy (Figure 2b).

## REFERENCES

[1] Baicheng Zhang, Nour-Eddine Fenineche, Lin Zhu,

- Hanlin Liao, Christian Coddet; Journal of Magnetic Materials, **324**, 495 (2012).
- [2] H.Ebrahimzadeh, S.A.A.A.Mousavi; Materials and Design, **38**, 115 (2012).
- [3] K.Gupta, K.K.Raina, S.K.Sinha; Journal of Alloys and Compounds, **429**, 357 (2007).
- [4] S.L.Dudarev, P.M.Derlet; J.Nuclear Materials, **251**, 367-370 (2007).
- [5] P.M.Derlet, S.L.Dudarev; Prog.Mater.Sci., **52**, 299 (2007).
- [6] J.Dalla Torre, Chu-Chun Fu, F.Willaime, A.Barbu, J.L.Bocquet; J.Nuclear Materials, **352**, 42 (2006).
- [7] S.L.Dudarev, P.M.Derlet; J.Phys.Condens.Matter., **17**, 7097 (2005).
- [8] Chu-Chun Fu, Jacques Dalla Torre, Francois Willaime, Jean-Louis Bocquet, Alian Barbu; Nature Materials, **4**, 68 (2005).
- [9] M.A.Vicente Alvarez, M.Marchina, T.Perez; Metallurgical and Materials Transactions A, **39**, 3283 (2008).
- [10] A.Seeger; Phys.Stat.Sol.(a), **167**, 289 (1998).
- [11] H.M.Li, D.Q.Sun, X.L.Cai, W.Q.Wang, Materials and Design, **39**, 285 (2012).
- [12] Fengxiao Huang, Zhonghao Jiang, Ximing Liu, JiansheLian, Li Chen; Journal of Materials Processing Technology, **209**, 4970 (2009).
- [13] Charles S.Montross, Tao Wei, Lin Ye, Graham Clark, Yiu-Wing Mai; International Journal of Fatigue, **24**, 1021 (2002).
- [14] Shihong Shi, AiqinXu, Jiwei Fan, Hongpu Wei; Nuclear Engineering and Design, **245**, 8 (2012).
- [15] C.Dimitrov, D.Huguenin, P.Moser, O.Dimitrov; J.Nucl.Mater., **147**, 22 (1990).
- [16] K.Ghazi-Wakili, Ph.Tipping, U.Zimmermann, W.B.Waeber; Z.Phys.B Condensed Matter, **79**, 39 (1990).
- [17] M.S.Anand, B.M.Pande; Phys.Stat.Sol.(a), **144**, 285 (1994).
- [18] E.Lima, Jr., V.Drago; Journal of Magnetism and Magnetic Materials, **280**, 251 (2004).
- [19] L.Coutu, L.Chaput, T.Waekerle; Journal of Magnetism and Magnetic Materials, **237**, 215-216,

- (2000).
- [20] R.Wurschum, E.A.Kummeler, K.Badura-Gergen, H.E.Schaefer; *Appl.Phys.*, **80**, 724 (1996).
- [21] K.Sumiyama; *Phys.Stat.Sol.(a)*, **126**, 291 (1991).
- [22] U.Brossmann, R.Wurschum, K.Badura-Gergen, H.E.Schaefer; *Phys.Rev.B*, **49(10)**, 6457 (1994).
- [23] H.E.Schaefer, R.Wurschum, J.Bub; *Mater.Sci.Forum*, **105**, 110 (1992).
- [24] H.E.Schaefer, B.Damson, M.Weller, E.Arzt, E.P.George; *Phys.Stat.Sol.(a)*, **160**, 531 (1997).
- [25] Y.A.Chang, L.M.Pike, C.T.Liu, A.R.Bilbrey, D.S.Stone; *J.Intermetal.*, **1**, 107 (1993).
- [26] A.R.Ali, F.Z.Ghobrial, E.Takla, K.K.Meleka; *Materials Science: An Indian Journal*, **13**, 108 (2015).
- [27] E.S.Gorkunov, S.M.Zadvorkin, S.V.Smirnov, S.Yu Mitropol'skaya, D.I.Vichuzhanin; *J.Physics of Metals and Metallography*, **103**, 311 (2007).
- [28] A.C.Damask, G.J.Dienes; "Point defects in metals", Gordon and Breach, New York, 148 (1963).
- [29] C.J.Meechan, J.A.Brinkman; *Phys.Rev.*, **103**, 1193 (1956).
- [30] O.Seydel, G.Froberg, H.Weaver; *Phys.Stat.Sol.(a)*, **144**, 69 (1964).
- [31] A.Refaat Ali, Z.M.Farid, F.Z.Ghobrial; *Z.Phys.B*, **94**, 227 (1994).
- [32] D.C.Jiles; *Phys.Stat.Sol.(a)*, **108**, 417 (1988).
- [33] O.Dimitrov, C.Dimitrov; *J.Nucl.Mater.*, **105**, 39 (1982).
- [34] S.Mantl, B.D.Sharma, G.Antesberger; *Phil.Mag.A*, **39**, 389 (1979).
- [35] A.I.Schindler, R.H.Kernohan, J.Weertman; *J.Appl.Phys.*, **35**, 2640 (1964).
- [36] M.S.Anand, B.M.Pande; *Phys.Stat. Sol.(a)*, **144**, 285 (1994).
- [37] A.Seeger, M.Kronmuller; *Mater.Sci.Forum*, **65**, 15118 (1987).
- [38] B.D.Sharma, K.Sonnenberg, G.Antesberger; *Phil.Mag.*, **377**, 777 (1978).
- [39] K.Nakata, S.Takamura, I.Masasak; *J.Nucl.Mater.*, **131**, 35 (1985).
- [40] G.Solt, W.B.Waeber, U.Zimmermann, Ph.Tipping, F.N.Gygax, B.Hitti, A.Schenk, P.A.Bearren; "Effect of radiation on materials", 14<sup>th</sup> International.Symposium, ASTM SPT 1046, Philadelphia, (1990).
- [41] A.R.Ali, Z.M.Farid, E.Takla; *Phys.Stat.Sol.(a)*, **128**, 295 (1991).
- [42] B.D.Cullity; "Introduction to Magnetic Materials", Addison-Wesley Publ.Co., 357, (1972).
- [43] H.Wagenblast, A.C.Damask; *J.Phys.Chem.Solids*, **33**, 221 (1962).
- [44] K.Ghazi-Wakili, U.Zimmermann, J.Bruneer, Ph.Tipping, W.B.Waeber, F.Heinrich; *Phys.Stat.Sol.(a)*, **102**, 153 (1987).